University of Washington Nuclear Physics Laboratory

Scaled Dimension Analysis and STAR Level-1 Trigger Algorithms

T. A. Trainor and J. G. Reid

Nuclear Physics Laboratory GL-10
University of Washington
Seattle, WA 98195

October 12, 1995

Ultrarelativistic Heavy Ions Group

1 Introduction

A previously developed autocorrelation and power spectrum analysis of 1-D multiplicity distributions [1] has been used to demonstrate a procedure for determining the 'distance' of a specific event from an ensemble of reference or 'normal' events in some representative pattern space. This distance measure can be used as the basis for various trigger criteria.

That approach was intuitive, and based on correlation measures then available to us. It served as a proof of principle but was not a substantive treatment of the underlying problem. Since that time we have developed a fundamental and comprehensive approach to the problem of correlation measurement which can now be applied to the level-1 trigger problem, and which does in our opinion provide a basic understanding of this problem and its optimum solution.

The new approach is based on a system of *scaled topological measures* of which the system of scaled Renyi entropies is central. We have determined [4, 5] that within this system *scaled dimension lowering* offers the most sensitive measure of differential correlation, and that this measure is actually closely related to the differential autocorrelation technique which we developed in our initial work. This is an unexpected but welcome confirmation of our earlier intuitive approach.

2 Differential autocorrelation analysis

2.1 Finite-domain autocorrelation

We assume that a nuclear collision event can be characterized in part by a set $\{n_i\}$ of particle multiplicity values corresponding to some finite, binned detector acceptance. The index i is the bin index. The definition of autocorrelation which we used in previous work [1] accommodates explicitly the bounded domain of the $\{n_i\}$ distribution

$$B_m = \frac{1}{M-m} \sum_{i=1}^{M-m} n_i \cdot n_{i+m}, \tag{1}$$

where M is the number of bins and N is the total multiplicity. These quantities are independent over the entire interval $m \in \{0, M-1\}$. This definition departs from the usual definition of autocorrelation used in signal analysis. The latter assumes that the finite data sample is part of an infinite periodic system, of which the sample comprises one period. We have determined that the autocorrelation A_m derived from this more restrictive definition is the *even* part of the quantity B_m defined above. The quantity B_m can be simply expressed in terms of the correlation integral as shown below, and is therefore closely related to fundamental topological quantities.

2.2 Differential autocorrelation

In our previous work we wanted to form a normalized differential quantity which would measure the departure of a given multiplicity distribution from an ensemble of 'normal' events. In the initial development of this technique [1] we generated events by assuming a uniform Poisson distribution as the norm, and then adding localized additional counts to form anomalous events. Thus, the normalized differential quantity was just the difference between the autocorrelation of the object distribution B_m and the autocorrelation for a Poisson distribution of the same total multiplicity

$B_{m,ref}$, divided by the latter quantity. This normalized differential autocorrelation was then given as

$$\begin{aligned} b_m &= (B_m - B_{m,ref})/B_{m,ref} \\ &= \frac{M-m}{M}(B_m/ < n >^2 -1 + 1/N - \delta_{m,0}/ < n >). \end{aligned} \tag{2}$$

In later work this technique was applied to modified HIJET events [2, 3], and the Poisson reference distribution was then no longer appropriate. A subset of the event population defined as (and intended to be) 'normal' events was instead used to form a quantity $b_{m,NH}$. A final differential quantity was then formed as

$$b'_m = b_m - b_{m,NH}. \tag{3}$$

This manipulation was carried out after the power spectra of the two correlations had been obtained. The quantity $b_{m,NH}$ or its power spectrum representation was referred to as the *null hypothesis* in this work. The null hypothesis concept is replaced in this and subsequent work by the *reference distribution.* This overall treatment was somewhat *ad hoc.* It could be defended in the case of small differences, but was not comprehensive.

3 Scaled topological measures

In more recent work [4, 5] we have concluded that the proper basis of relative correlation measurement is the degree of *scaled dimension lowering* in magnitude and scale of a given distribution compared to some reference distribution which may represent a constraint system (this is closely related to the partition-function approach in statistical mechanics). The degree of correlation is measured relative to this reference distribution. The scaled dimension lowering $\Delta d_q(e)$ with respect to some reference distribution is a general and model-independent measure of the degree of relative correlation in the (object) distribution of interest.

The system of scaled topological measures which we have developed is based on the concept of scaled, dithered binning. Bin contents derived from a scaled binning of the object distribution are combined to form certain measures, of which the Renyi entropies and dimensions are most important. Comparing the measures for the object distribution and for a reference distribution we extract scaled dimension lowering distributions. We further transform these distributions as described below to form the coordinates of pattern spaces which may serve as the basis for a trigger system. In this section we describe the scaled Renyi entropy and dimension system.

3.1 Renyi entropy

Using a normed representation $p_i(e) = n_i(e)/N$ of the i^{th} bin contents we can approximate the scaled rank-q correlation integral as

$$C_q(e) = \sum_{i=1}^{M_1(e)} p_i^q(e). \tag{4}$$

In terms of the correlation integral we can also write the scaled rank-q Renyi entropy as

$$\begin{aligned} S_q(e) &= \frac{1}{1-q} log[C_q(e)] \\ &= \frac{1}{1-q} log[\sum_{i=1}^{M_1(e)} p_i^q(e)], \end{aligned} \tag{5}$$

where $M_1(e)$ is the number of bins containing at least one point in the case of a discrete distribution. The first few entropies can be written explicitly as

$$\begin{aligned} S_1 &= -\sum_i p_i log(p_i) \\ &= -< log(p) > \\ S_2 &= -log < p > \\ S_3 &= -log < p^2 >^{1/2}, \end{aligned} \tag{6}$$

and so forth, where $<>$ here represents an average over the bin system with respect to the normed weight set $\{p_i\}$. $S_1(e)$ is the Gibbs entropy.

3.2 Scaled dimension

We define the scaled rank-q set dimension in terms of the corresponding Renyi entropy as

$$d_q(e) = -\frac{dS_q(e)}{dloge}. \tag{7}$$

The quantities S_0 and d_0 are illustrated in fig. 1 for a 1-D Poisson distribution. L represents the size of the bounded space in which the distribution is contained, and the scale is represented by e. The scaled dimension is zero at large scale because the bounded distribution appears point-like. At very small scale the dimension again approaches zero because the individual points of the distribution are resolved at these scales. Over some scale interval the dimension approaches that of a uniform distribution in the 1-D embedding space. This interval depends on the size of the boundary L and the number of points N.

3.3 Scaled dimension lowering

We define the scaled rank-q information as

$$I_q(e) = S_q(e) - S_{q,ref}(e), \tag{8}$$

where $S_{q,ref}(e)$ is the reference entropy for the system, representing some reference distribution. The accurate determination of $S_{q,ref}$ in a given circumstance is a critical and sometimes difficult task.

The scaled information as defined here is an exponential representation of *volume reduction*, since entropy is an exponential representation of volume. This definition of information accommodates the conventional perception that receipt of information results in a reduction of the number of alternative representations of a given system. A set of alternative representations is equivalent to

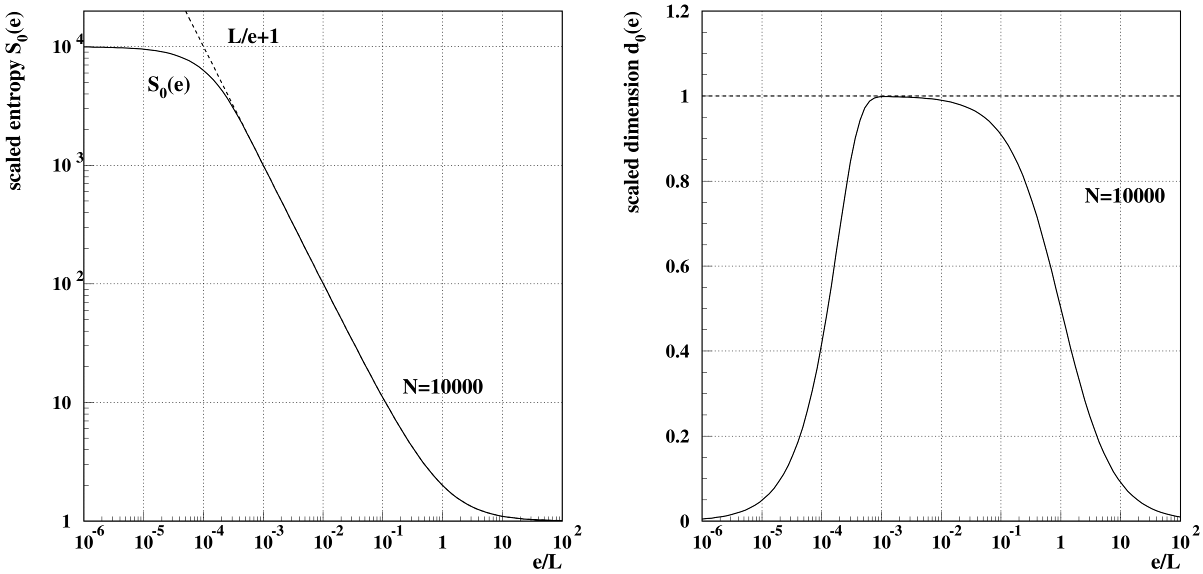

Figure 1: Scaled rank-0 entropy and dimension for 1-D Poisson distribution

a certain volume in a representational space. Thus, receipt of information is equivalent to volume reduction and should be measured accordingly.

We define dimension lowering in terms of scaled information as

$$\begin{aligned}\Delta d_q(e) &= -\frac{dI_q(e)}{dloge} \\ &= -\frac{dS_q(e)}{dloge} + \frac{dS_{q,ref}(e)}{dloge} \\ &= d_q(e) - d_{q,ref}(e). \end{aligned} \tag{9}$$

This quantity is intended to measure as sensitively as possible the increase (or decrease) in correlation of an object distribution in comparison to a reference distribution. Dimension lowering is a model-independent *differential* measure of correlation. These properties make it a key element in a complex trigger system, in which we search for events whose correlation content (morphology) is significantly different from a select population of 'normal' events.

4 Relationship between the two analysis systems

4.1 Autocorrelation and correlation integral

The finite-domain autocorrelation was given in eqn. 1 by

$$B_m = \frac{1}{M-m} \sum_{i=1}^{M-m} n_i \cdot n_{i+m}. \tag{10}$$

The relationship between the bin index m and the scale parameter e is as follows. The index m labels a set of M 'microbins' used in the autocorrelation analysis. These bins are of fixed size measured by some parameter ϵ (= L/M) and should not be confused with the scaled bin system measured by the parameter e and used to evaluate topological measures. In the following approximation the scale e for the correlation integral $C_q(e)$ takes on discrete values $e_m = m \cdot \epsilon$ corresponding to the microbin centers. Therefore, we can write $B_m = B_2(e_m)$.

The quantity $B_m \cdot (M - m)$ is the total number of pairs with size (separation) *between* e_m and e_{m+1}. Given that the correlation integral $C_2(e_m)$ is the number of pairs with size *less than* e_m normalized to the total number of pairs $N^{[2]}/2$ ($N^{[q]} = N!/(N-q)!$) we can approximate the scale derivative of the correlation integral by

$$\begin{aligned} dC_2(e_m)/de_m &\approx \Delta C_2(e_m)/\Delta e_m \\ &\approx \frac{2B_m \cdot (M-m)}{N^{[2]} \cdot \epsilon} \\ &\approx \frac{2B_2(e_m) \cdot (L - e_m) \cdot M^2}{N^{[2]} \cdot L^2}. \end{aligned} \tag{11}$$

As noted in eqn. 5 the scaled rank-q Renyi entropy can be expressed in terms of the correlation integral by

$$S_q(e_B) = \frac{1}{1-q} log[C_q(e_B)]. \tag{12}$$

These two expressions, with $q = 2$, relate the finite-domain autocorrelation to the Renyi-entropy-based scaled topological measure system.

There is a subtlety contained in these relationships. The correlation integral derived from the autocorrelation has as its domain of integration a 'tube' of some radius e coaxial with the main diagonal in a 'pair space' formed from a cartesian product of two primary spaces (the object distribution is represented in 'primary' space). On the other hand, the scaled topological measures are predicated on a binning of the primary space. The corresponding domain of integration for the correlation integral in this latter case is a set of nonoverlapping bins of size e along the main diagonal in pair space. The scale (radius) for the tubular domain we represent by e_m, while the scale (bin size) for the binning approach we represent by e_B. The relationship between the two quantities which insures a consistent treatment is given by

$$e_B = 2e_m \cdot (1 - \frac{e_m}{2L}). \tag{13}$$

The expression in egn. 11 relates to the autocorrelation, and so the scale is measured by e_m. To make a full correspondence with the system of topological measures based on a scaled binning system we must transform to the parameter e_B. Carrying out this transformation we obtain

$$dC_2(e_B)/de_B \approx \frac{B_2(e_m) \cdot M^2}{N^{[2]} \cdot L}. \tag{14}$$

As a simple example, consider the case of a Poisson distribution, with autocorrelation given by the expression

$$B_2(e_m) = \frac{N^{[2]}}{M^2}. \qquad m \neq 0 \tag{15}$$

The derivative in scale of the correlation integral becomes in this case

$$dC_2(e_B)/de_B \approx \frac{1}{L}. \tag{16}$$

From here we drop the subscript B. By a trivial integration this gives the correlation integral for the Poisson distribution as

$$C_2(e) = e/L. \tag{17}$$

In deriving this expression we have neglected dithering, which becomes important when $e \approx L$. A full dithered binning analysis would result in the expression

$$\begin{aligned} C_2(e) &= \frac{e}{L}(1 - \frac{e}{3L}) \quad e/L < 1 \\ &= 1 - \frac{L}{3e} \quad e/L > 1. \end{aligned} \tag{18}$$

Using eqn. 5 we find that the corresponding Renyi entropy is

$$\begin{aligned} S_2(e) &= log[L/e] - log[1 - e/3L] \quad e/L < 1 \\ &= -log[1 - L/3e] \quad e/L > 1. \end{aligned} \tag{19}$$

This expression is the expected rank-2 entropy for a Poisson distribution above some scale value for which the finite point number is no longer a significant factor. This is consistent with the implicit assumption for eqn. 15 that the mean microbin occupancy is significantly greater than unity.

4.2 Differential autocorrelation and dimension lowering

We earlier took as our differential measure of correlation [1] the normalized difference

$$b_m = \frac{B_m - B_{m,ref}}{B_{m,ref}}. \tag{20}$$

An improved differential measure of correlation, to which this is an approximation, is

$$log[B_2(e_m)/[B_{2,ref}(e_m)] \approx b_m. \tag{21}$$

Using our previous results we now carry out the following steps

$$\begin{aligned} B_2(e)/B_{2,ref}(e) &= \frac{dC_2(e)/de}{dC_{2,ref}(e)/de} \\ &= \frac{C_2(e)}{C_{2,ref}(e)} \cdot \frac{dlog[C_2(e)]/dloge}{dlog[C_{2,ref}(e)]/dloge} \\ &= \frac{C_2(e)}{C_{2,ref}(e)} \cdot \frac{d_2(e)}{d_{2,ref}(e)}. \end{aligned} \tag{22}$$

Taking the logarithm of both sides we have

$$\begin{aligned} log[B_2(e)/[B_{2,ref}(e)] &= log[C_2(e)] - log[C_{2,ref}(e)] + log[d_2(e)/d_{2,ref}(e)] \\ &= -I_2(e) + log[d_2(e)/d_{2,ref}(e)]. \end{aligned} \tag{23}$$

We can now relate the normalized differential autocorrelation to the rank-2 scaled information lowering. For small differential correlation the second term of this expression can be approximated by

$$log[d_2(e)/d_{2,ref}(e)] \approx \Delta d_2(e)/d_{2,ref}(e). \tag{24}$$

Using eqn. 9 we then obtain in the limit of small differential correlation

$$b_m \approx \left(\int dloge + \frac{1}{d_{2,ref}(e)} \right) \cdot \Delta d_2(e). \tag{25}$$

The integral part of the operator acting on the dimension lowering $\Delta d_2(e)$ is an effective bandwidth limitation when we make an FT of the dimension lowering to wavenumber space. Thus, it can be argued that the dimension lowering by itself is superior to the differential autocorrelation as a measure of differential correlation. Furthermore, while this particular expression relates the differential autocorrelation (pair correlation) to the scaled topological measure system for $q = 2$, these results also permit an extension of differential correlation analysis to the complete range of q values in the Renyi entropy system, thus considerably expanding the capability of such analysis.

To summarize, in the original autocorrelation analysis technique we used a differential measure of correlation b_m which approximated $log[B_2(e)/[B_{2,ref}(e)]$. In our subsequent scaled dimension lowering analysis we have used the quantity $\Delta d_2(e)$. In this section we make clear the relationship between these two quantities. They are closely related, with the $\Delta d_2(e)$ measure having a superior capability because of the elimination of the bandwidth-limiting integral term and because through this model treatment the complete range of q values becomes accessible for this type of analysis.

5 Standard set of anomalous events

We hope for qualitatively new QCD physics at RHIC. Thus, we must create a trigger system for STAR which is both highly specific and adaptive, with as much flexibility as possible to respond to newly acquired results in an optimum fashion. In order to move forward with this task we need a system of simulated event data which both represents the standard behavior (presently) anticipated for relativistic nuclear collisions and contains the possibility to simulate various kinds of anomalous behavior in a controlled manner, so that the capabilities of trigger algorithms can be fully tested.

An initial set of special Monte Carlo (MC) events has been generated by Ron Longacre of BNL to provide a basis for testing trigger algorithms[6]. This set consists of four groups of 100 events each, labeled rhic, landau, chiral and smoke. These names refer in some way to the models used to generate anomalous rearrangement of energy, and therefore particle production, in the test events. The rhic events are the reference events, and are derived from a modified version of HIJET which uses the N-N CM system and corrects the treatment normally given in HIJET to leading diquarks in terms of flavor changing and stopping (transparency).

Landau events are a modification of earlier Van Hove plasma bubble events. For Van Hove events a fraction of the total collision energy goes into formation of one or more plasma bubbles. These then expand isotropically and deflagrate into thermal hadrons which are thereby localized in rapidity, forming one or more local particle excesses. In the Landau modification this expansion is not isotropic, but is modified to agree with Bjorken longitudinal expansion recently confirmed at SPS energies. This expansion model results in smoother structures in rapidity than previously obtained with the original plasma bubble events.

Smoke events are similar to Landau events except that the deviation from Van Hove plasma bubbles is not from isotropic to longitudinal but from isotropic to transverse expansion, resulting in sharper structures in the rapidity distribution. This alternative is intended to be more an exercise to test algorithmic systems than an anticipation of possible new physics.

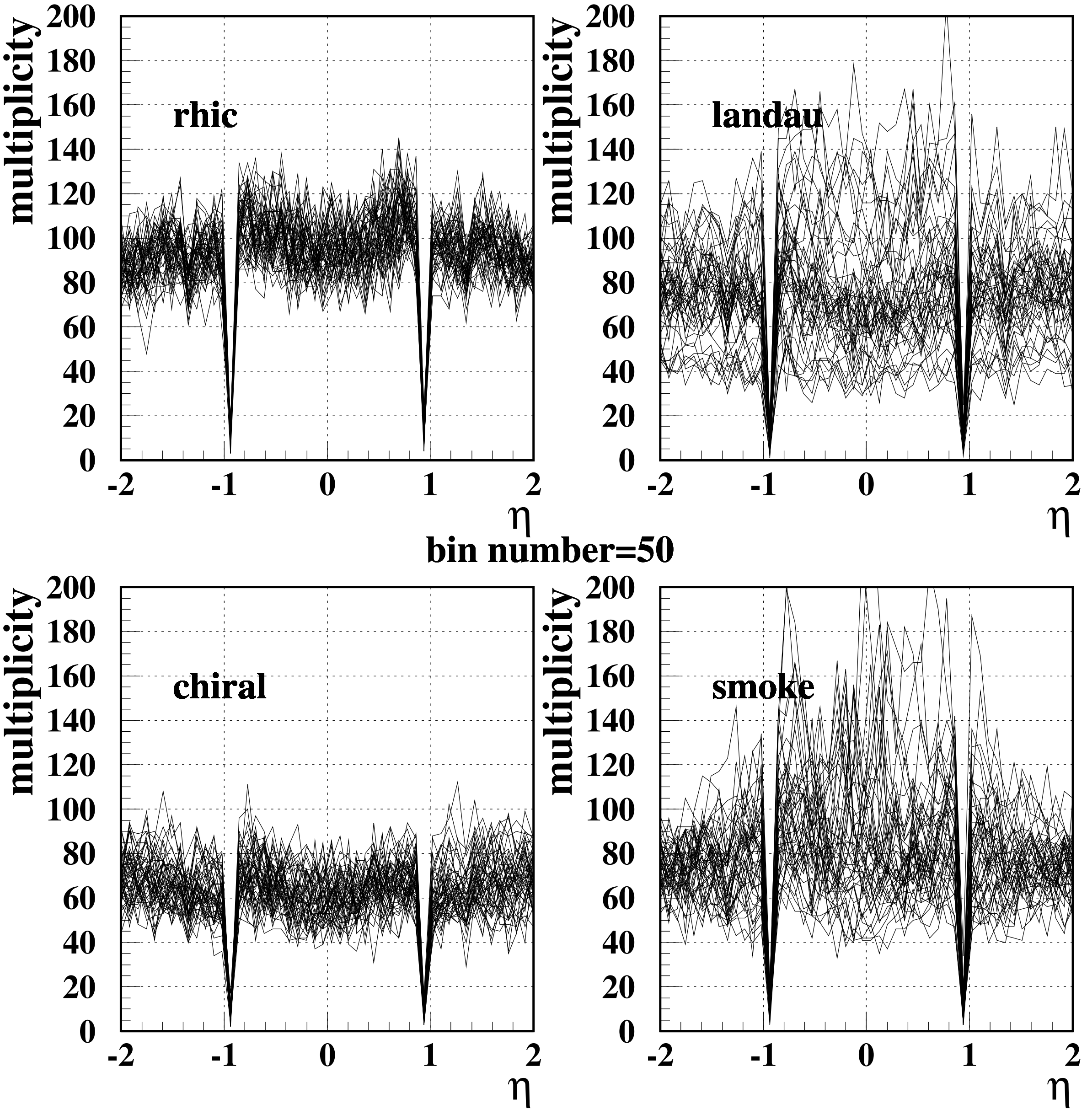

Figure 2: Multiplicity distributions with 50 equal bins.

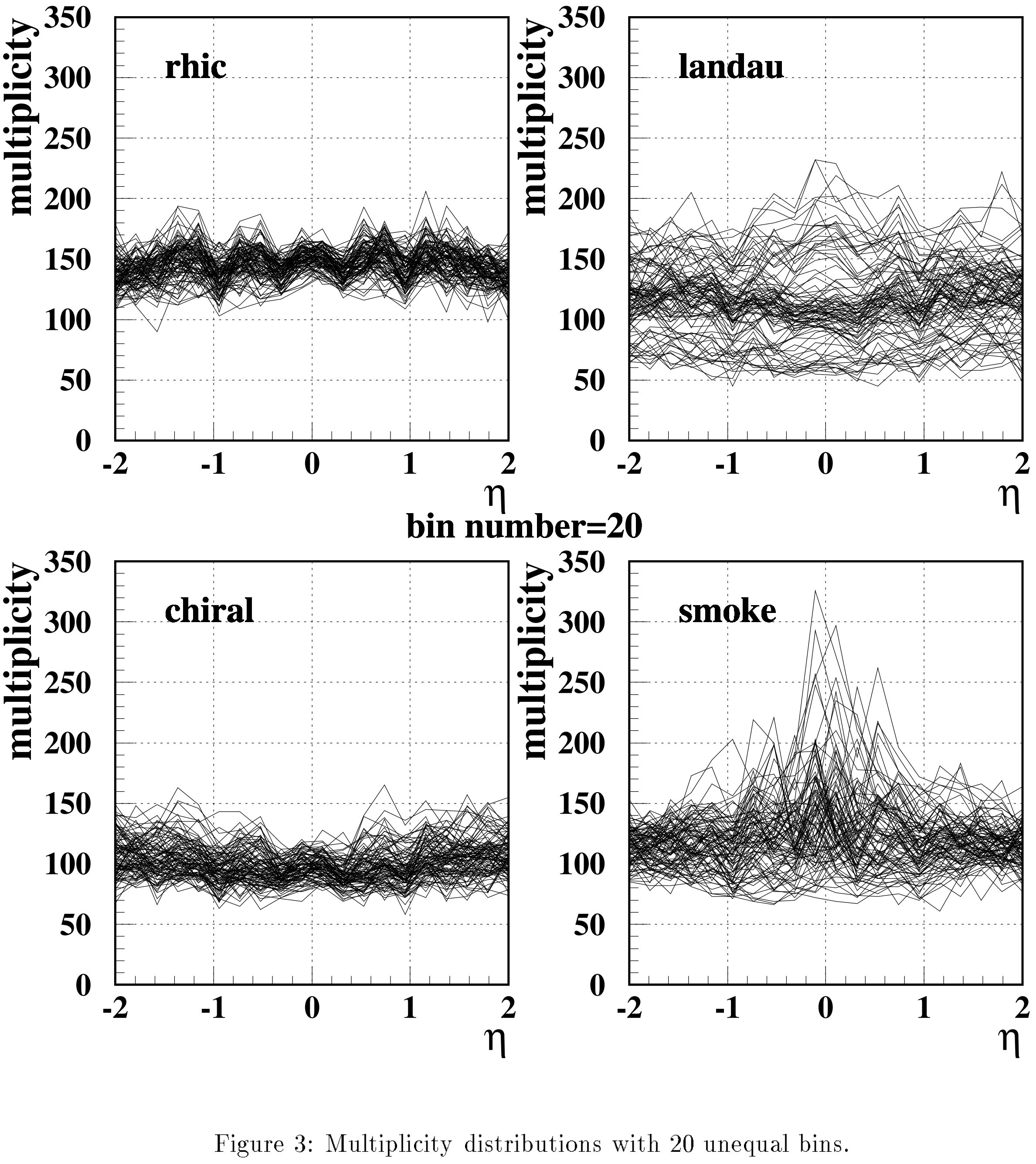

Figure 3: Multiplicity distributions with 20 unequal bins.

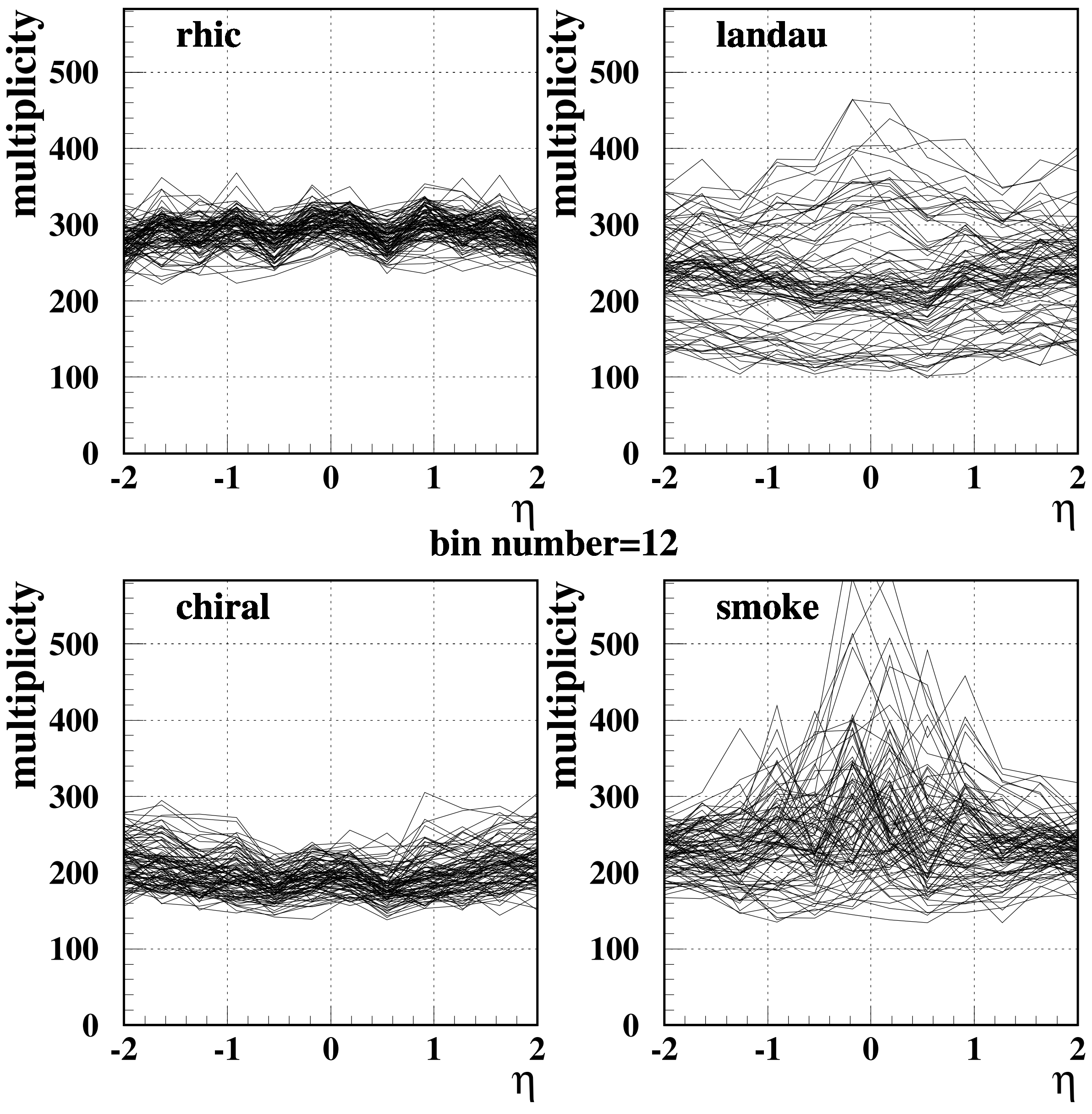

Figure 4: Multiplicity distributions with 12 equal bins.

Chiral events are meant to simulate the nonuniformities in charged particle distributions that might arise as the result of formation of a disoriented chiral condensate. These events are again based on the Van Hove bubble model, but with the bubble isospin distribution (and therefore charged-to-neutral pion ratio) departing significantly from the normal binomial distribution with mean 1/3.

As a minimum-correlation reference we have also generated 100 Poisson events, each with a total multiplicity equal to the mean multiplicity of the rhic events.

Four event sets are shown for three different binning schemes in figs. 2 - 4. The fifty-bin and twelve-bin distributions have uniform bin width throughout the acceptance. The twenty-bin distributions have nonuniform binning systems. The central four bins cover the eta interval [-1,1] with four bins. the other sixteen bins cover the eta ranges [-2,-1] and [1,2] in sets of eight bins each. The multiplicities in the central four bins have been divided by four for the plots in fig. 3

The fifty-bin distributions preserve all relevant correlation information in the original hit distributions. The obvious gaps in these distributions correspond to a hiatus in coverage between trigger detector components. The twenty-bin distribution models the actual STAR trigger detector complement and the 12-bin distribution is included to study the effect of information loss by coarse binning.

6 Scaled dimension-lowering results

Here we show two sets of dimension lowering distributions for the five event types. In fig. 5 we show the distributions over a broad scale interval [-2.8,1], and in fig. 6 we show the same distributions over a restricted scale interval [-1,0] meant to correspond to the coarsest binning case (10 bins) conceivable.

Recall that $log(e/L) = 0$ in these plots corresponds to the full acceptance. In fig. 5 the structure near the smallest scale ($log(e/L) < -2$) corresponds to event-wise variations in total multiplicity. This is because the total multiplicity within a fixed acceptance determines the point density, and therefore the scale at which individual points are resolved. One can see in this figure that the total multiplicity for the rhic events shows little variation, the total for the chiral events is systematically and uniformly lower than that for the rhic events, and the landau and smoke events show substantial fluctuations in total multiplicity. This behavior can be confirmed directly in fig. 2.

Because the total event multiplicity is already used as a trigger criterion in level 0 we do not want to be sensitive to this quantity in the level-1 analysis. Therefore, we restrict the scale interval of our analysis to lie above -1.7, thus conservatively eliminating the effects of the multiplicity variations contained in these distributions.

It is notable that $10^{-1.7} = 1/50$. Thus, our chosen lower limit on the scale interval corresponds to the 50-bin system in figure 2. The 12-bin system on the other hand corresponds to a scale interval lower limit of -1.08. We carry out correlation analyses over both [-1.7,0] (fine) and [-1,0] (coarse), thereby bracketing all anticipated binning schemes.

The reference distribution for all but the poisson1 dimension lowering is represented by the rhic event ensemble-averaged scaled entropy. For poisson1 the refence distribution is the poisson event ensemble average. We see in subsequent results a similarity therefore between poisson1 and rhic, since these populations are both being compared to their own population averages as reference. The difference between the poisson1 and rhic results reveals the variance contained in the rhic events which exceeds Poisson statistics and results from other statistical processes in the HIJET event generator.

Having obtained these distributions the question remains how best to represent the correlation information contained in them for trigger purposes. With the finite bandwidth of the level-1 trigger processors and the very short time interval available to form a decision, a rather rudimentary version of this correlation analysis will be necessary at level 1, with accompanying loss of information. The question of the best compromises for formation of trigger criteria and algorithms within this finite computational bandwidth will be left to another report.

We consider here the extraction of the *maximum* amount of correlation information from these multiplicity distributions with the complete scaled dimension lowering technique, and the compromise to that process by more or less restrictive trigger detector binning. These results will then serve as a standard for comparison as we restrict the correlation analysis to accommodate the limitations of the level-1 trigger system in further study. At higher levels of the trigger system more complete versions of the correlation analysis become possible, and the full correlation analysis is certainly desirable in a final data analysis.

For the present work we use a Fourier transform approach. Selected elements of the power spectrum resulting from an FT of the dimension lowering distribution are used in varying combinations to form the parameters of trigger or pattern spaces. This process is described in more detail in the next section.

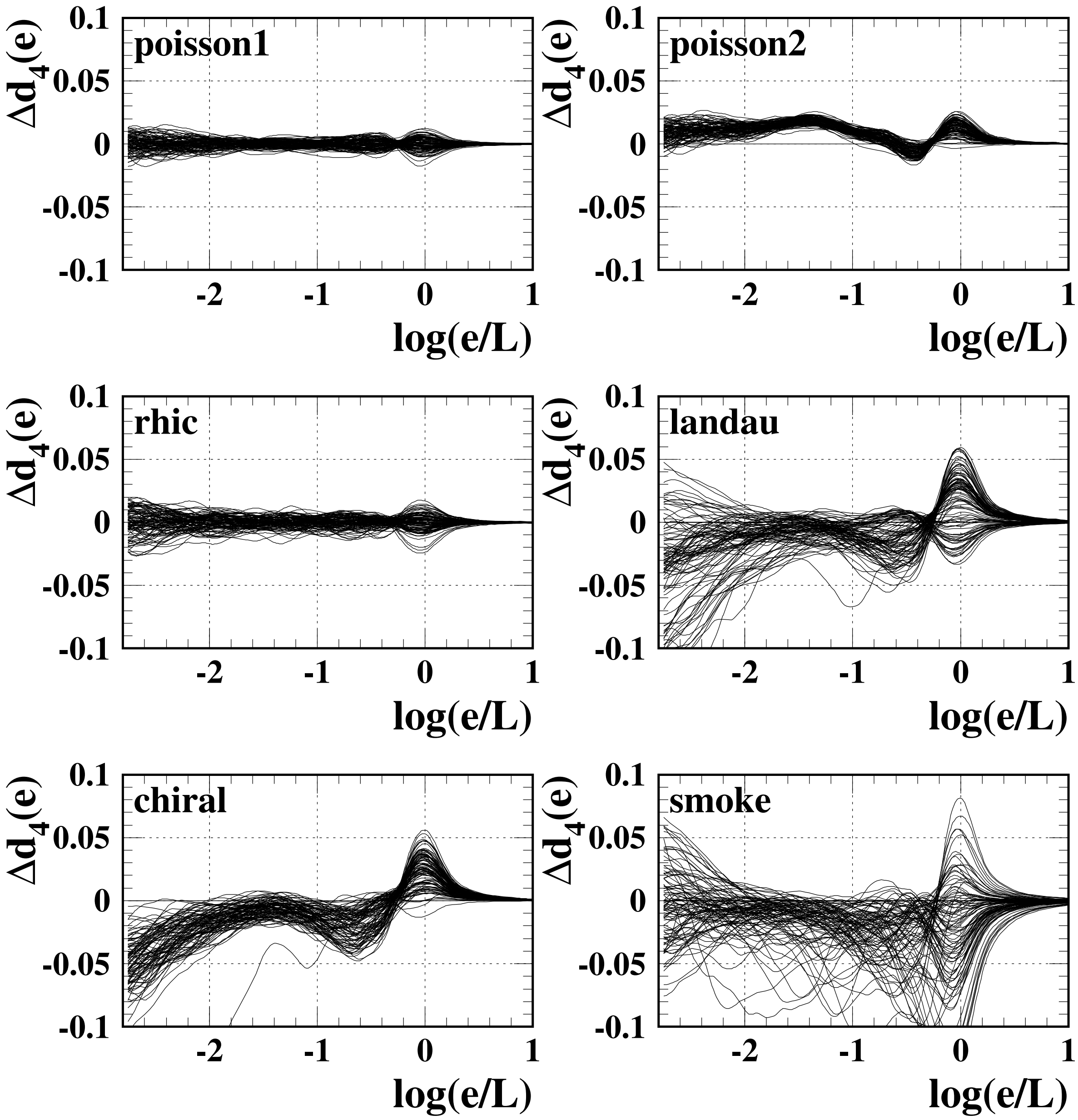

Figure 5: Scaled dimension lowering over full scale window.

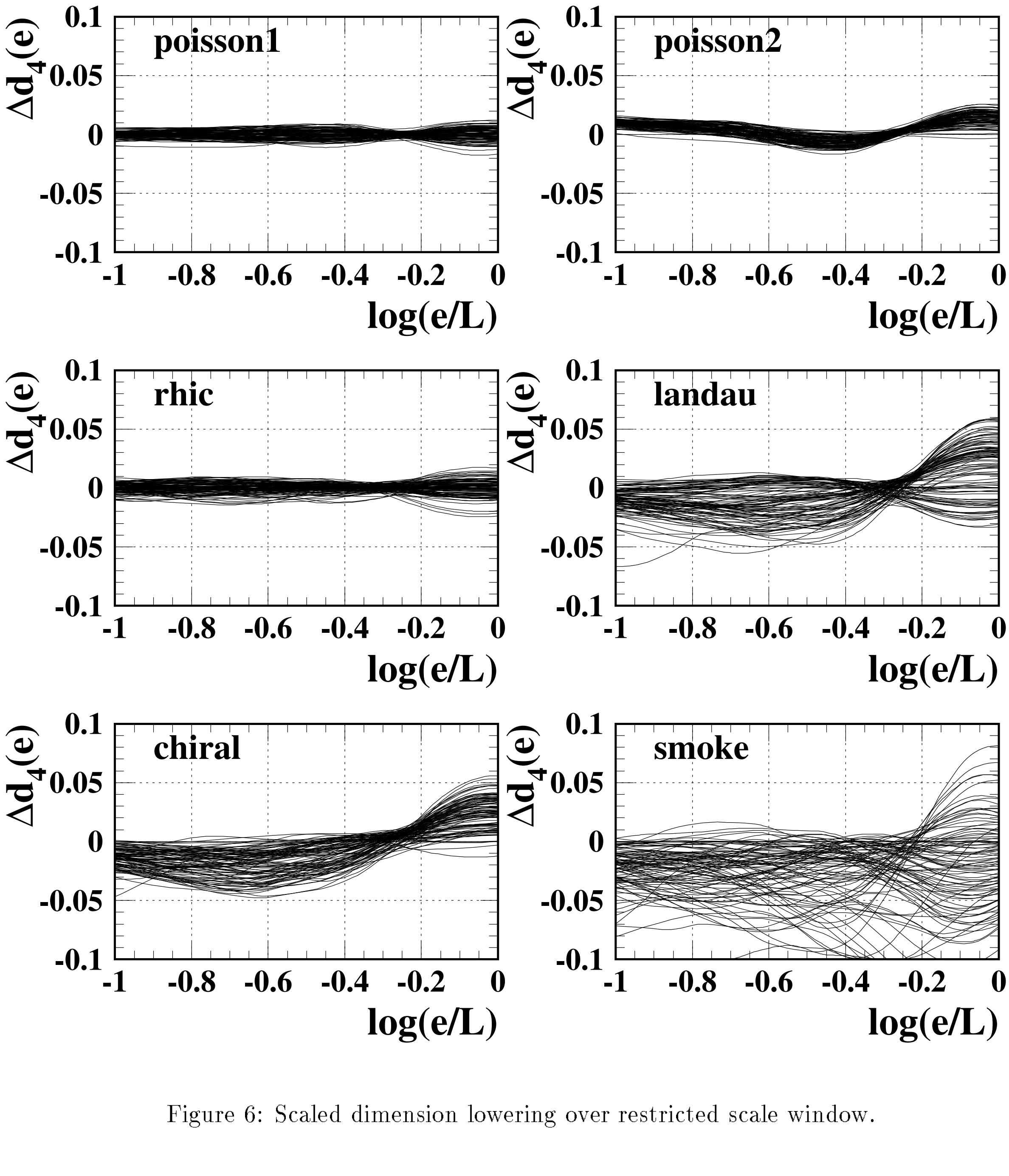

Figure 6: Scaled dimension lowering over restricted scale window.

7 Power spectra

The dimension-lowering distributions shown in fig. 5 and 6 are evaluated at each of M=59 scale points with a step size of $log_{10}[1.2]$. Suppressing the rank index q in what follows we can in general write the discrete Fourier transform (FT) of the dimension lowering as

$$\Delta \hat{d}_k = \frac{1}{M} \sum_{j=1}^{M} \Delta d_j \cdot e^{-\mathbf{i}\frac{2\pi}{M}k \cdot j} \tag{26}$$

with the inverse

$$\Delta d_j = \sum_{k=1}^{\hat{M}} \Delta \hat{d}_k \cdot e^{\mathbf{i}\frac{2\pi}{M}j \cdot k}. \tag{27}$$

For our present application we restrict the sum in eqn. 26 to the equivalent scale interval $log(e/L) \in [-1.7, 0]$ so as to exclude the level-0 event multiplicity information in this level-1 analysis. We use the real and imaginary parts of the FT to form the magnitudes

$$\hat{P}_k = \sqrt{((Re\Delta\hat{d}_k)^2 + (Im\Delta\hat{d}_k)^2)} \tag{28}$$

and phases

$$\hat{\Phi}_k = atan2((Re\Delta\hat{d}_k, Im\Delta\hat{d}_k) \tag{29}$$

of the power spectrum. These quantities are plotted in fig. 7, with the phase being the oscillatory quantity.

One can see that there is a great deal of information in these phase spectra. In searching for the most complete and efficient representation of the morphological event information in these distributions we have obtained second-stage (sel = 2) power spectra of the first-stage (sel=1) phase spectra shown in fig. 7. These second-stage power spectra are shown in fig. 8. Here one sees that the different event types are further split into a number of subgroups. We will study the relationship between these phase spectra and various event morphologies below.

From the first-stage power spectra we extract the total power

$$P = \sum_{k=1}^{\hat{M}} \hat{P}_k. \tag{30}$$

In addition we choose specific elements from the phase spectra which seem best able to discriminate among event types and subtypes. This is not at this time a well-defined procedure. In the next section we show results with phase spectrum components from first- and second-stage FTs and compare the degree of selectivity with these various quantities.

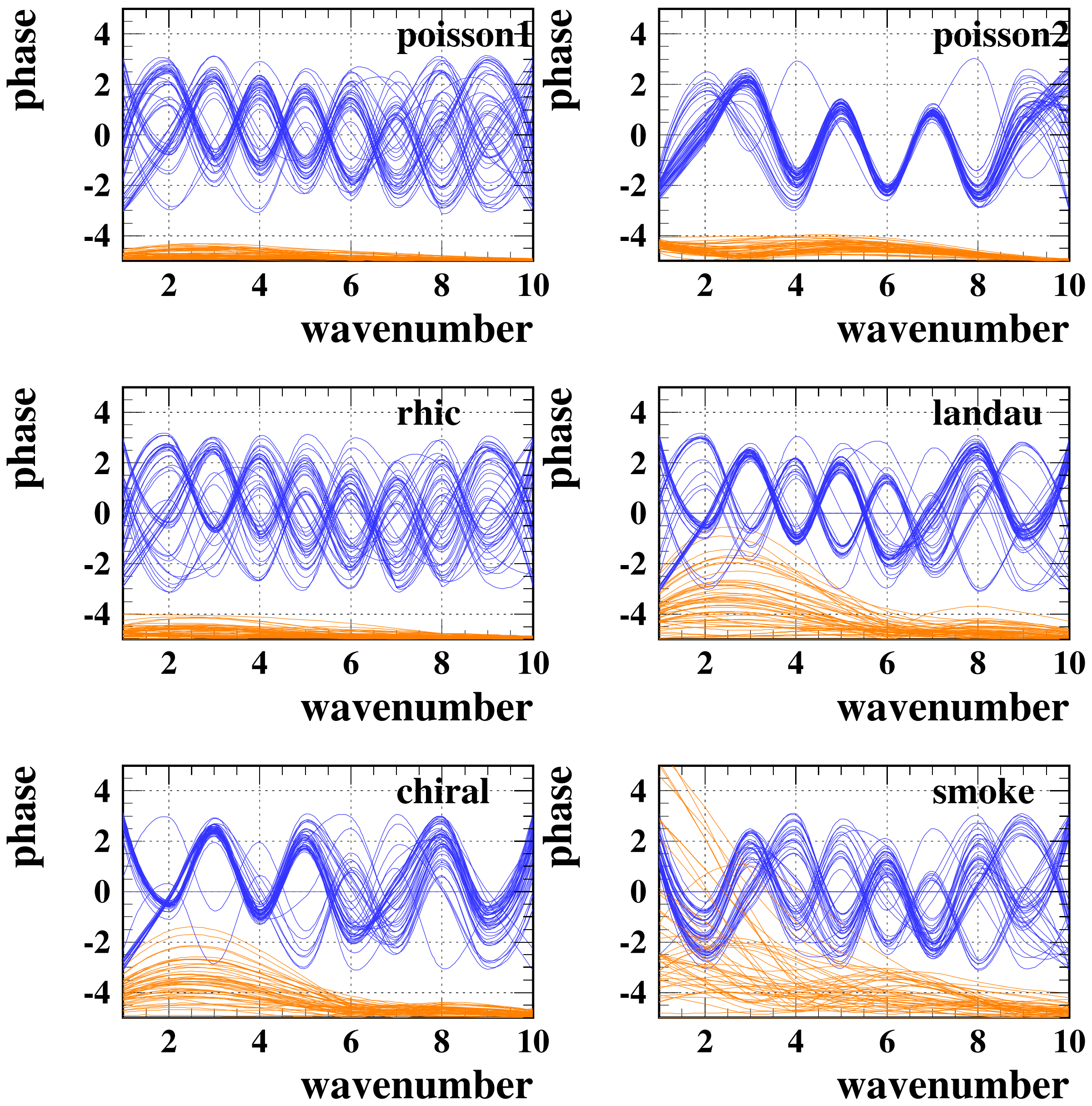

Figure 7: First-stage Fourier spectra for rank-4 dimension lowering.

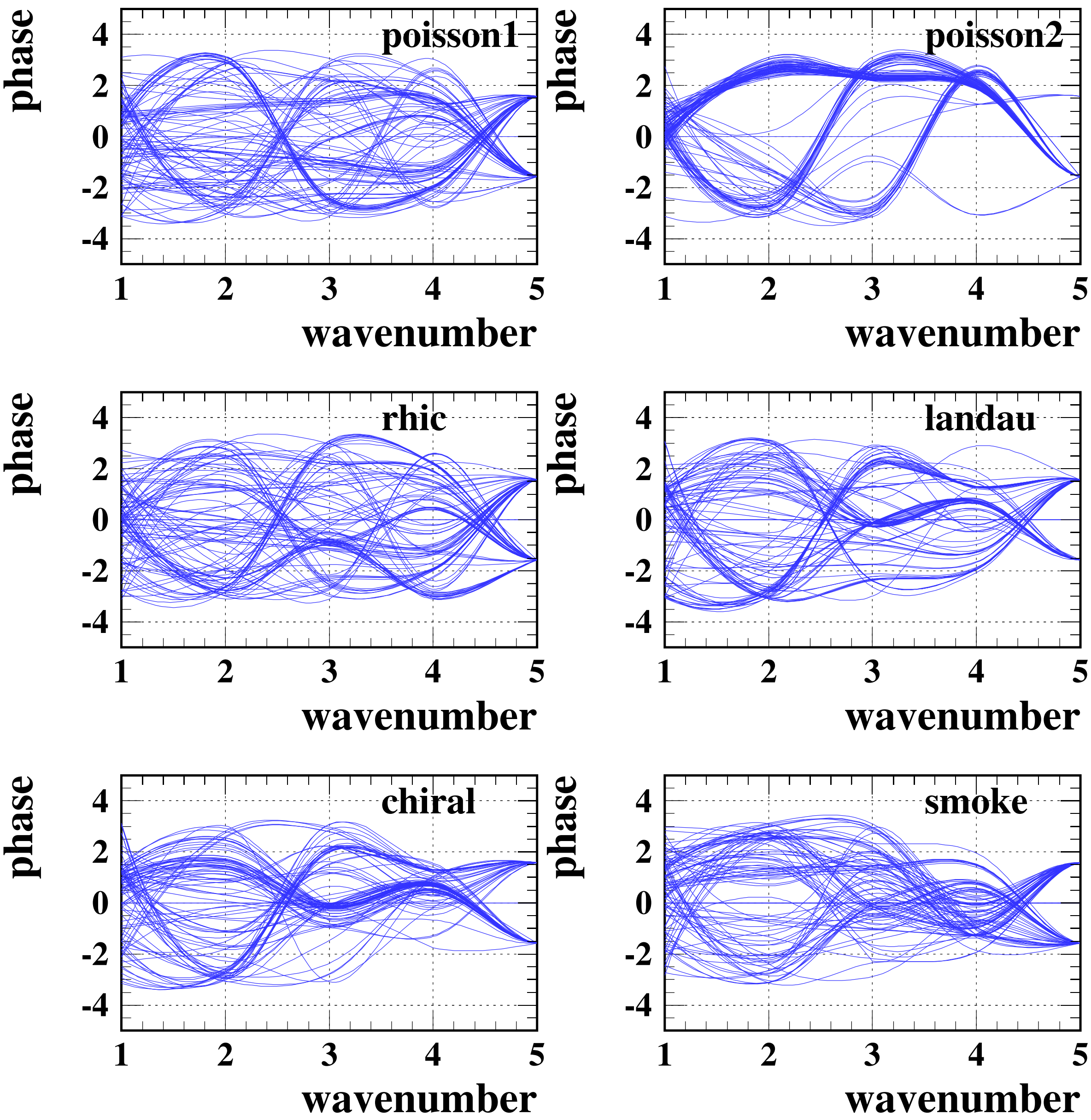

Figure 8: Second-stage Fourier spectra for rank-4 dimension lowering.

8 Formation of pattern spaces

The general strategy at this time for the formation of pattern or event selection spaces is to use various combinations of the total power and selected elements of the phase spectra shown in the previous section for each event to form two- and three-dimensional spaces in which event selection can be performed. These phases are obtained from the primary FT spectra (sel=1) and from secondary FT spectra obtained in turn from the primary FT spectrum phase distribution (sel=2).

A sel=1 pattern space can be characterized by the wavenumber indices (k) of the three phase values used. For instance the label 279 would indicate that $\hat{\Phi}_2$, $\hat{\Phi}_7$ and $\hat{\Phi}_9$ (cf. eqn. 29) were used to form the coordinates of the pattern space. Unless otherwise noted the sel=2 pattern space is 234.

Given these primary variables for pattern space formation there are several ways that they can be combined. Most generally, three coordinates can be formed from the power and three primary phases as $P \cdot \hat{\Phi}_{k_1}$, $P \cdot \hat{\Phi}_{k_2}$ and $P \cdot \hat{\Phi}_{k_3}$. Four views of this space for 279 are shown in figs. 9 (sel=1) and 10 (sel=2). One can see that different event morphologies tend to cluster around processes radiating from the origin. This indicates that a modified space could be formed by considering this space as a spherical polar coordinate system, thereby reducing the variable number from four to three. The derived variables are then power and the two phases

$$\phi = atan2(\Phi_{k_3}, \Phi_{k_2}) \tag{31}$$

and

$$\theta = atan\left(\frac{sin(\phi) \cdot \Phi_{k_1}}{\Phi_{k_3}}\right). \tag{32}$$

Plots of this space for sel = 1, 2 are shown in figs. 11 and 12.

To carry out event selection we need to specify subvolumes or zones in these spaces. For initial study it is convenient to specify the subvolumes in a 2-D space defined by the two derived phases θ and ϕ. The power can be constrained to be above some lower limit, within a range, or not specified at all. Such a 2-D space for sel=1 is shown in fig. 13. Also shown in this figure is a set of zones labeled A through I which will be used to examine event selection in the next section.

Finally, for quick 2-D examination of power vs phase we can derive a third phase by considering the space in fig. 13 to be a polar system, with polar phase angle ψ defined by

$$\psi = atan2(\phi, \theta). \tag{33}$$

A comparison of this space for sel=1, 2 is shown in fig. 14. This space can also be used for event selection, but the discrimination among events is naturally less effective.

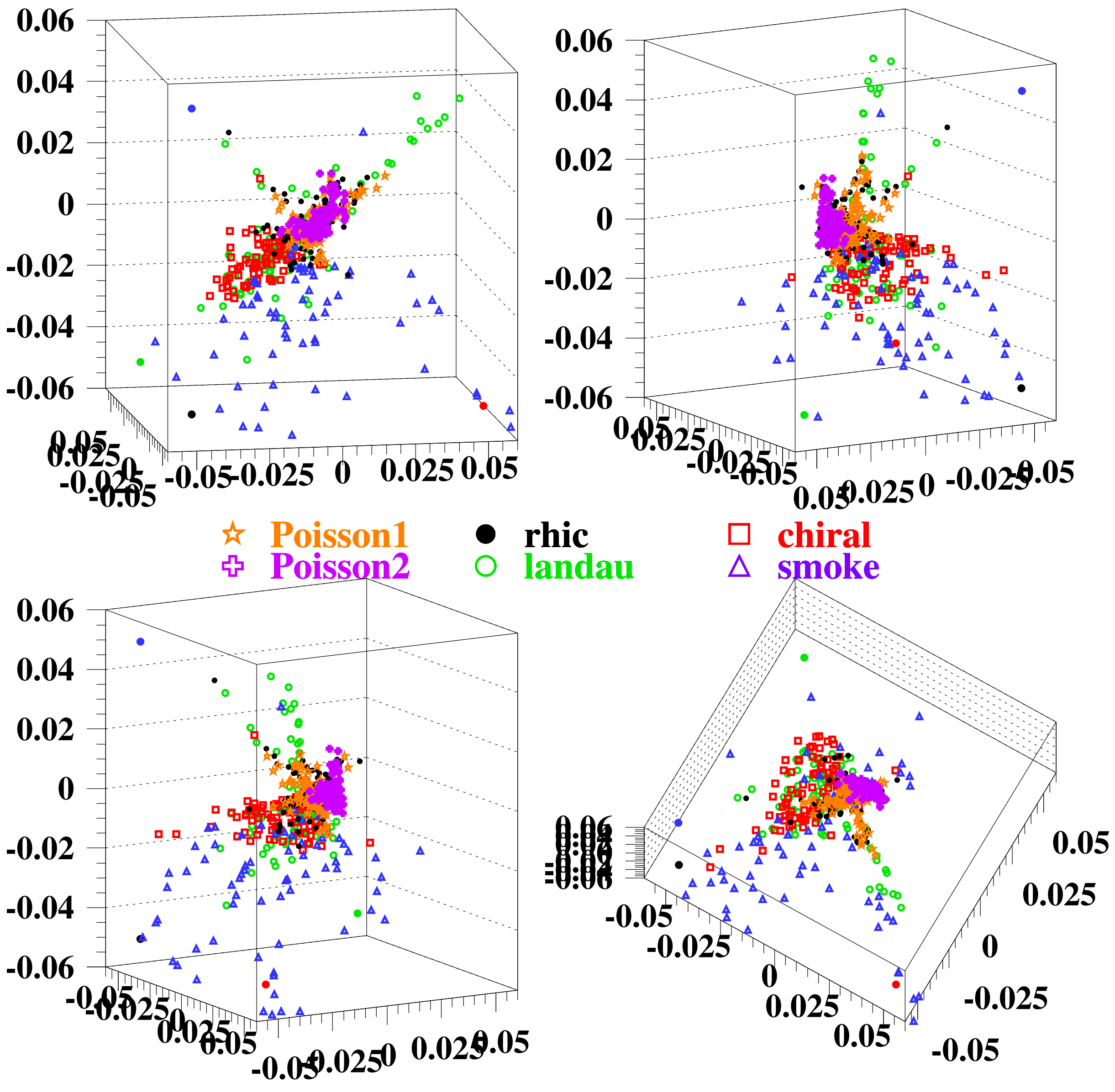

Figure 9: First-stage three-phase pattern space.

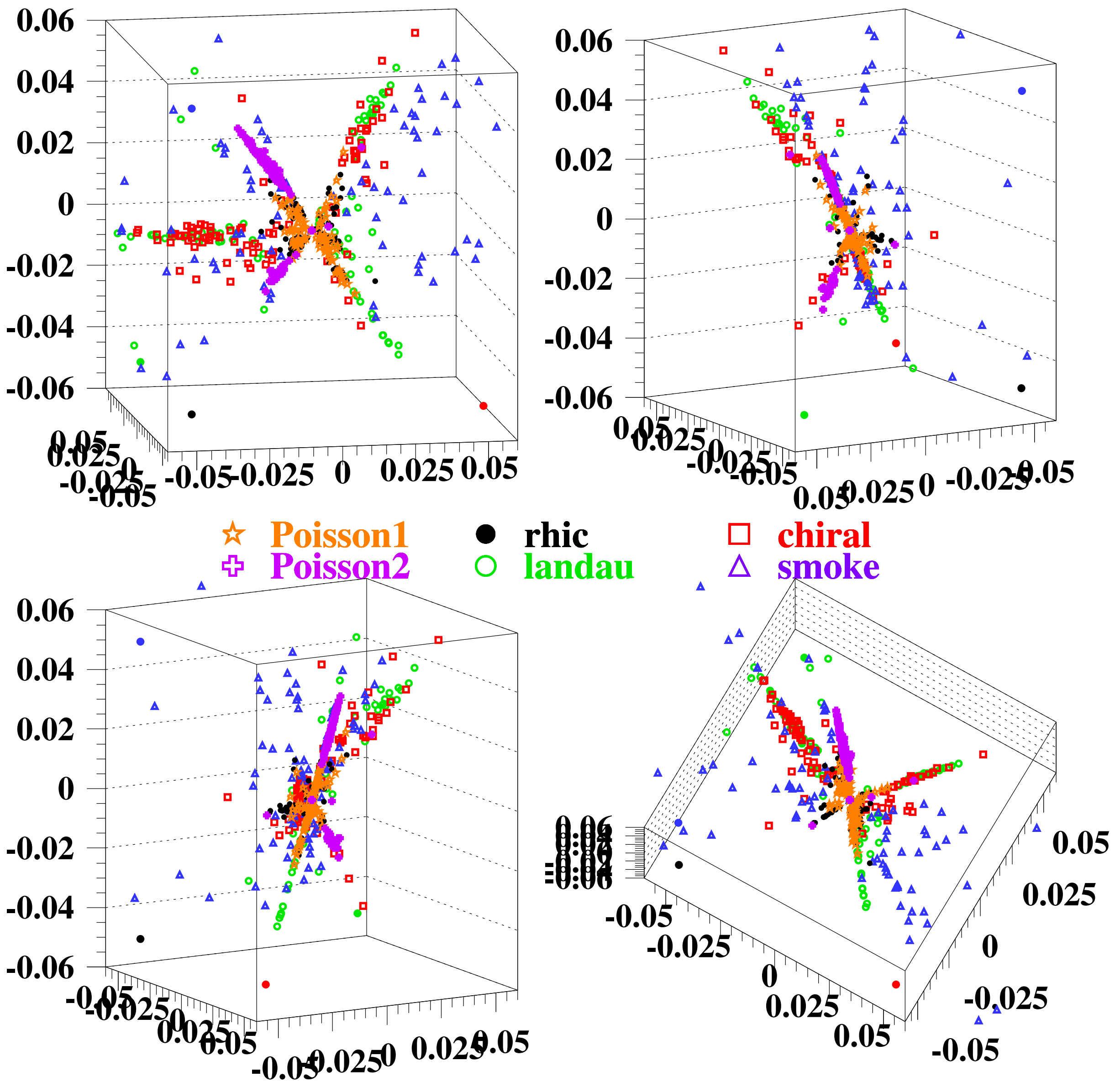

Figure 10: Second-stage three-phase pattern space.

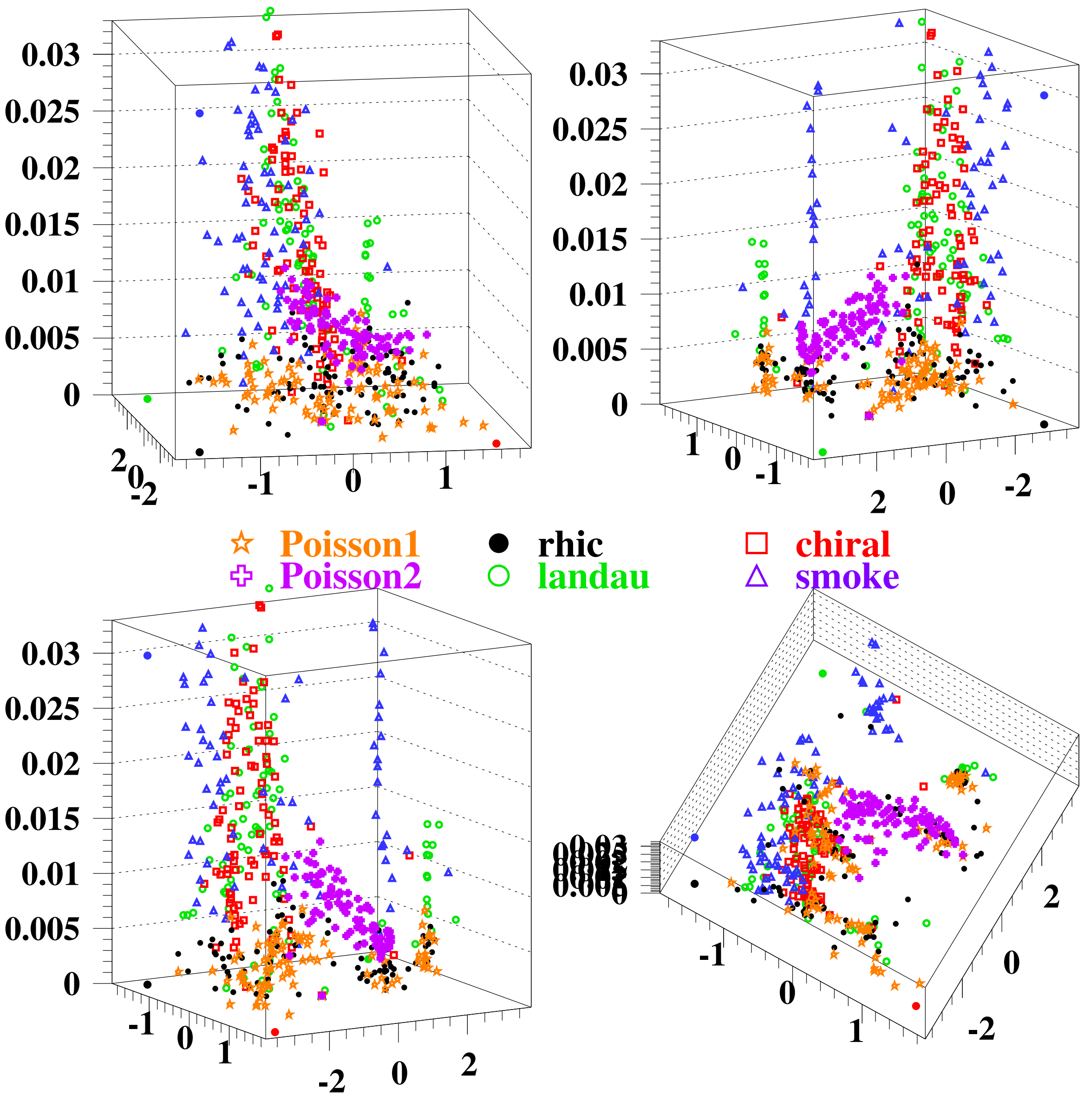

Figure 11: First-stage two-phase pattern space.

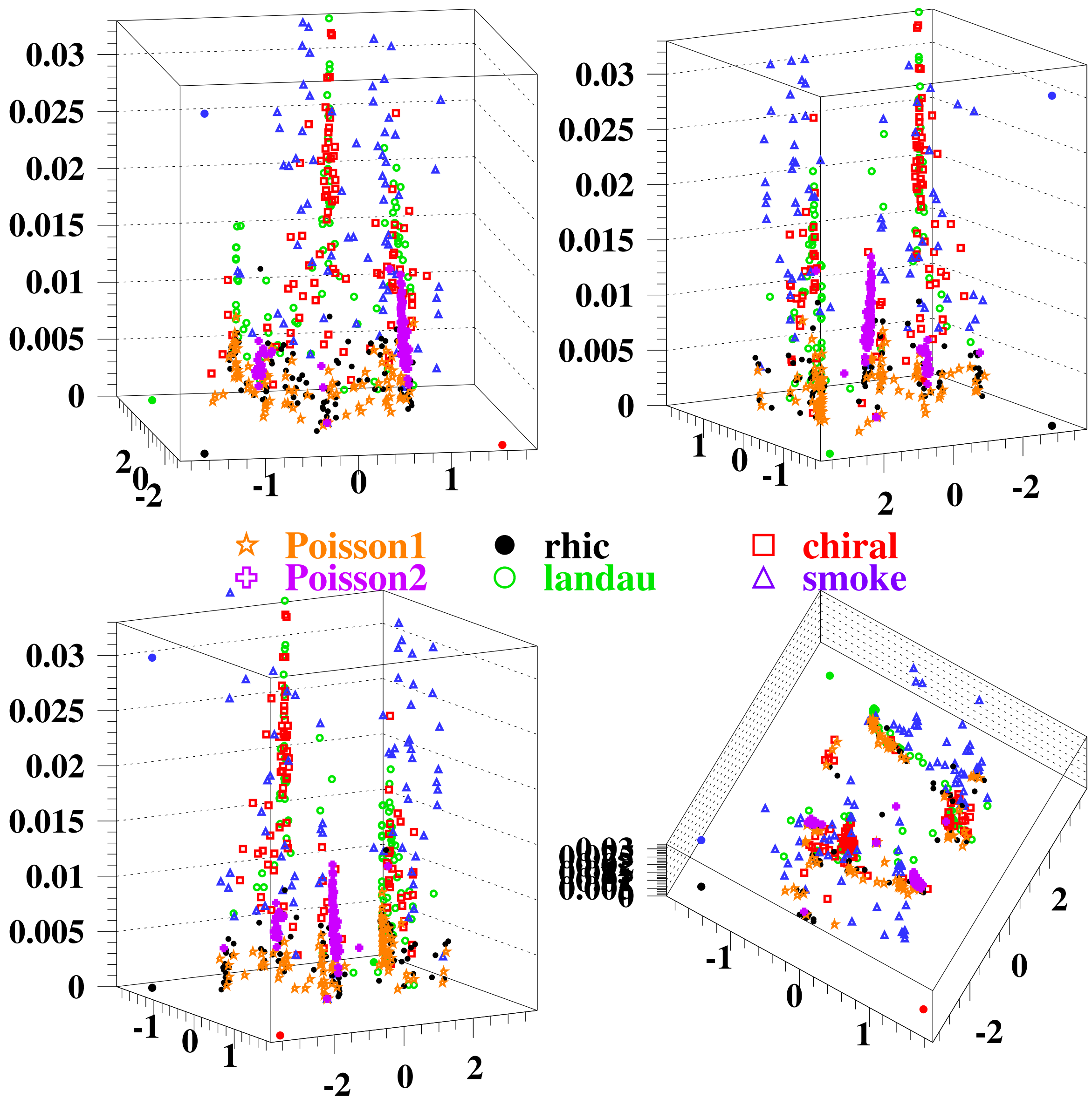

Figure 12: Second-stage two-phase pattern space.

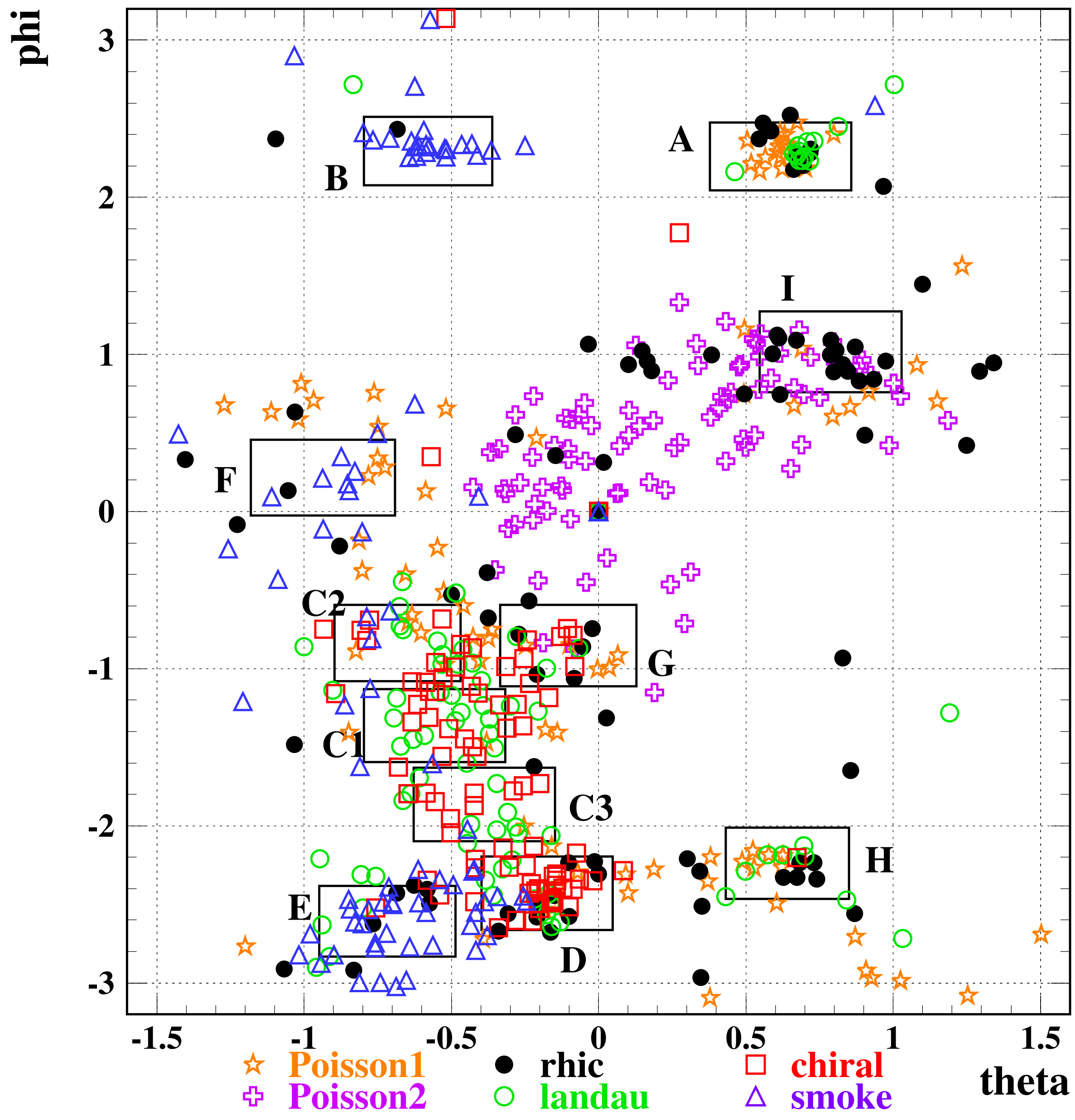

Figure 13: Projected first-stage two-phase pattern space showing event selection zones.

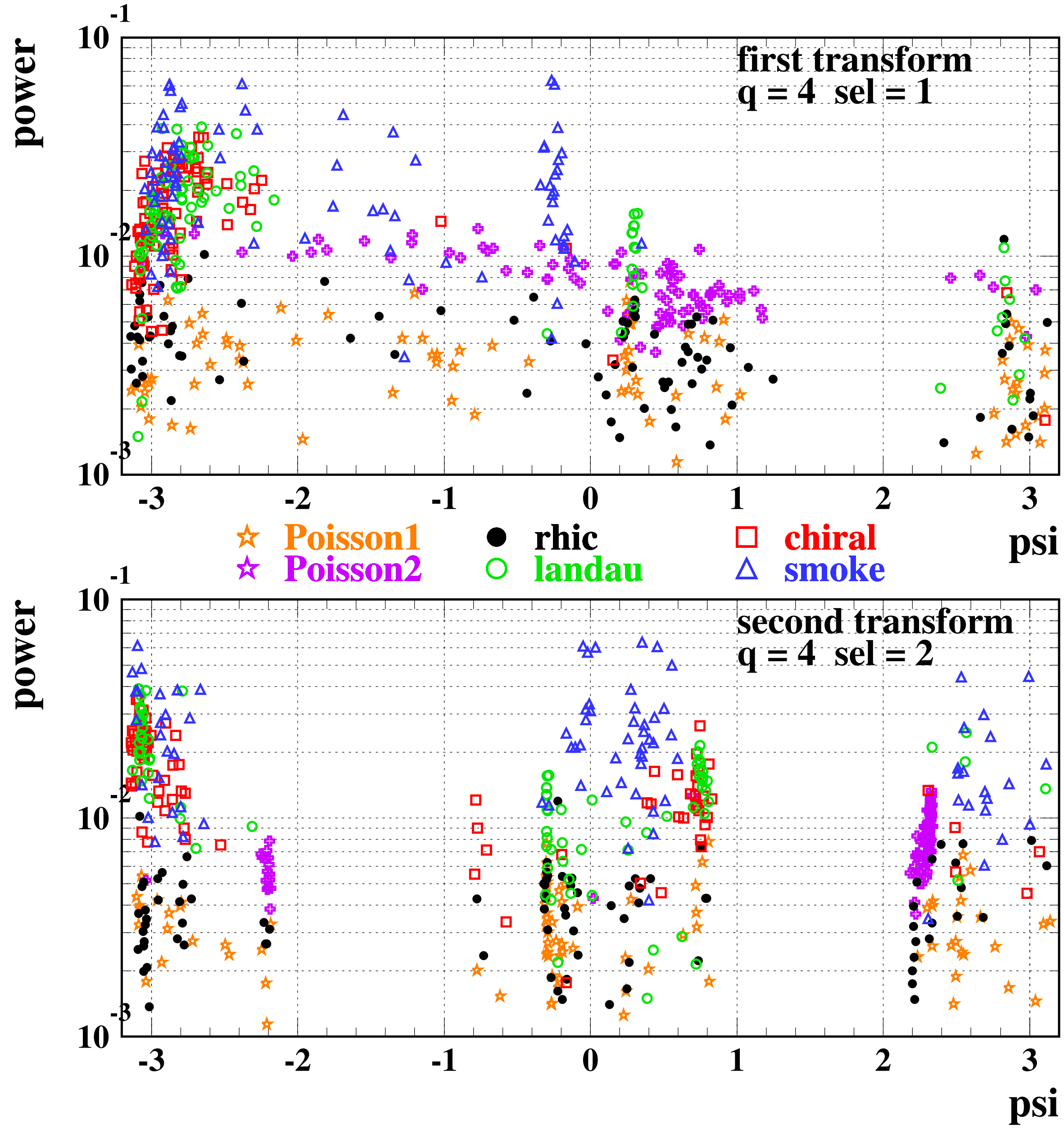

Figure 14: First- and second-stage single-phase pattern spaces.

9 Event selection performance

For this demonstration of principle and in view of the rather small event sample we have placed a simple lower limit on power at 0.001 (cf. fig. 14). This means that there is essentially no discrimination based on the amplitude of an anomaly, only on shape. In this way all of the events within a 2-D selection zone in fig. 13 are visualized.

The multiplicity distributions are plotted in this section with bin density normalized to unity, so as to eliminate any apparent differences due to total multiplicity variation. Three general terms can be used to characterize the morphologies of this event population: concave, convex and detailed structures. The zones C1, C2, C3 and D select populations of generally concave events, with some detailed structure. In zone C2 (fig. 15) we see a central, almost rectangular dip superposed on a general concave distribution. In zone C1 (fig. 16) the central dip is hardly noticeable. In zone C3 (fig. 17) the distribution is smoothly concave and in zone D (fig. 18) the distribution is developing a central peak, especially for smoke events.

In zone G (fig. 19) the distributions are nearly flat, with some evidence of structure toward the ends of the distribution. In zone E (fig. 20) the distribution is dominated by a sharp central peak for smoke events. The grouping with the other events in this case is not understood.

In zone H (fig. 21) we see the transition to a convex distribution. In zone F (fig. 22) we see a continuation from zone C2 of the trend to a central, box-like depression. But in the case of zone F this has advanced to the formation of two peaks on either side of the central region.

In zone B (fig. 23) we have a transition to a very strongly peaked central region with neutral background. In zone A (fig. 24) we see a smoothly convex distribution with a tendency to a central peak, whereas in zone I (fig. 25) there is no sign of a central peak, but still overall the distribution is convex.

Recalling that fig. 13 is part of a periodic system we can see that zones B and E are closely related, selecting events with a strong central peak, whereas zones midway between, such as C1 and C2 select for central dips. Zones to the left (B, E, F, negative theta) seem to select for sharp structures whereas zones to the right (A, I, H, positive theta) select for broad structures. We can begin to see therefore the systematic trends in such a pattern space by this simulation procedure.

These exercises serve mainly to illustrate the selective power of this technique for events which might be expected with the STAR trigger detector system in level 1. This somewhat simplified application has not employed the full discriminative power of the technique so that we might provide a clearer picture of the process. Selection on power level and full 3- or higher-dimensioned spaces are obvious extensions of the method. These elaborations require a much larger anomalous event sample.

10 Conclusion

We have developed a system of scaled topological measures and applied them to 1-D multiplicity distributions in order to form selection or pattern spaces which may be used to discriminate among events according to their morphologies, independent of the total event multiplicity. This system shows excellent selection capability, and reveals nontrivial structural details not apparent to the eye.

This study should serve as a reference for further trigger design. We extract here the maximum amount of morphological information from these events without regard to analysis or cpu time.

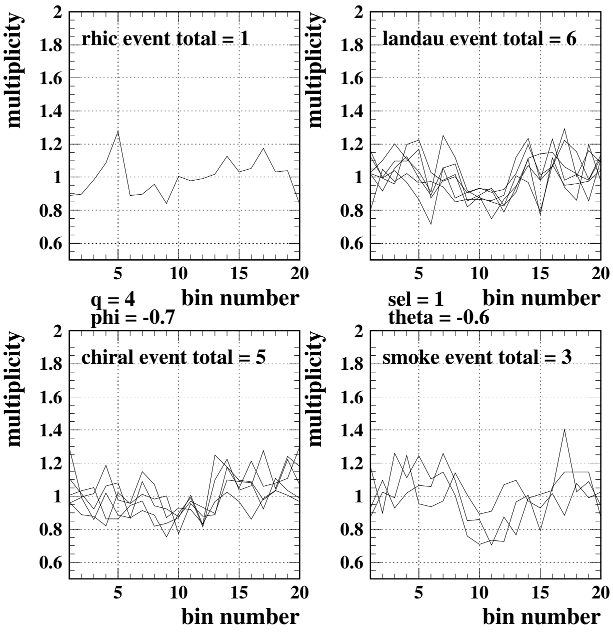

Figure 15: Zone C2

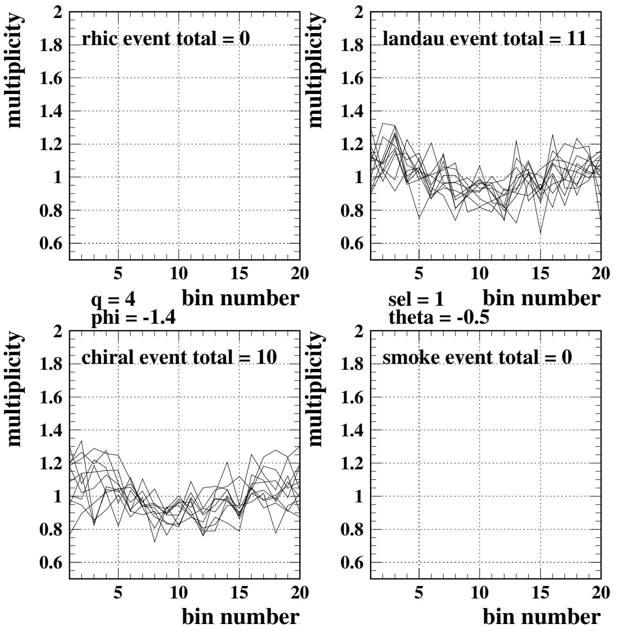

Figure 16: Zone C1

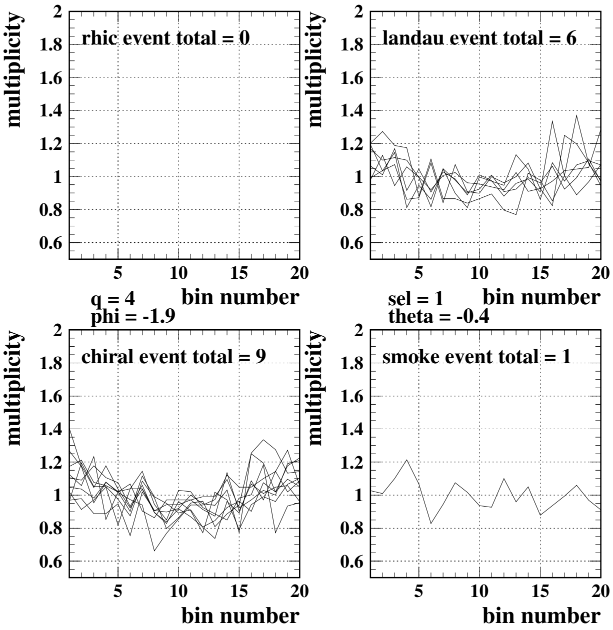

Figure 17: Zone C3

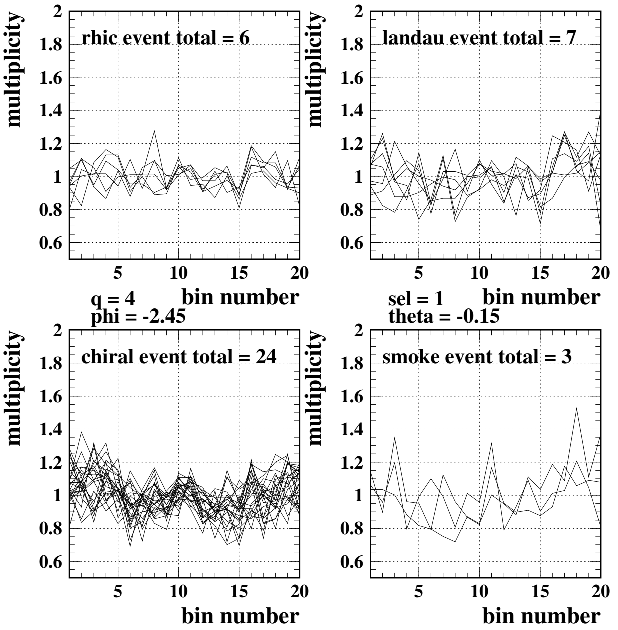

Figure 18: Zone D

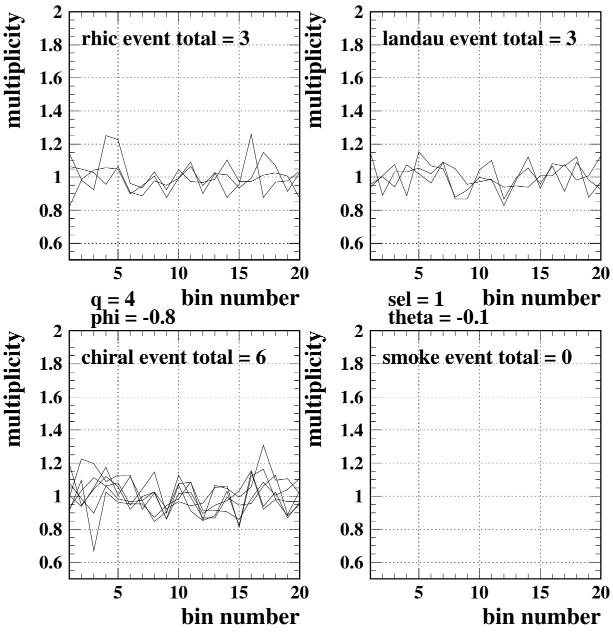

Figure 19: Zone G

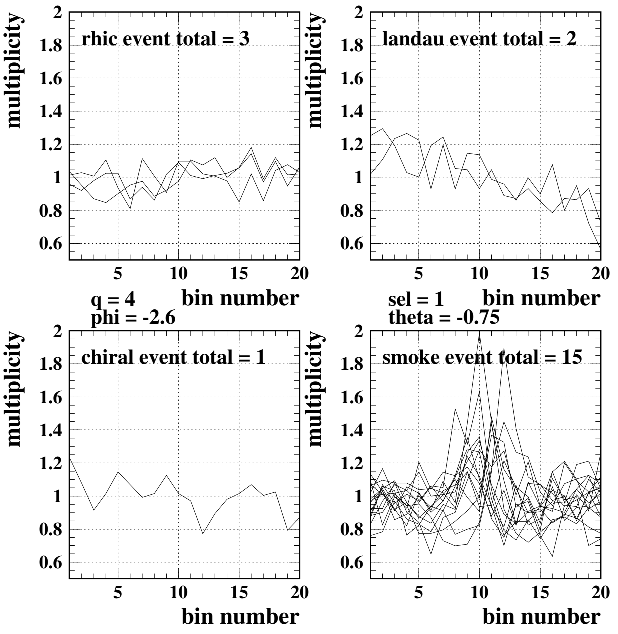

Figure 20: Zone E

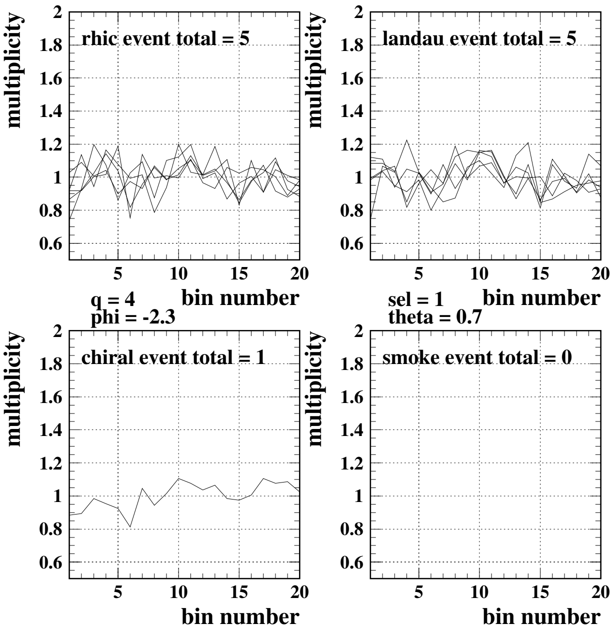

Figure 21: Zone H

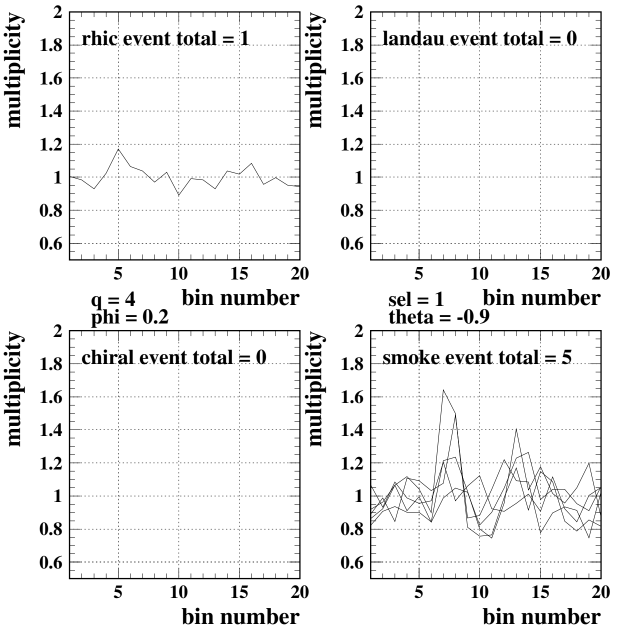

Figure 22: Zone F

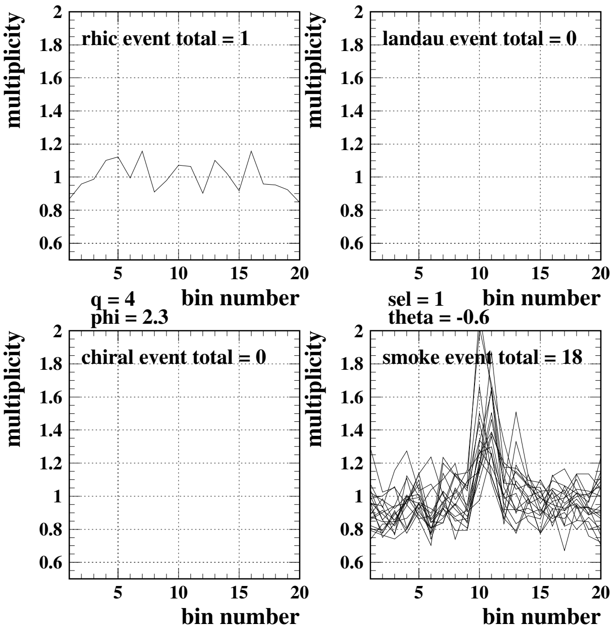

Figure 23: Zone B

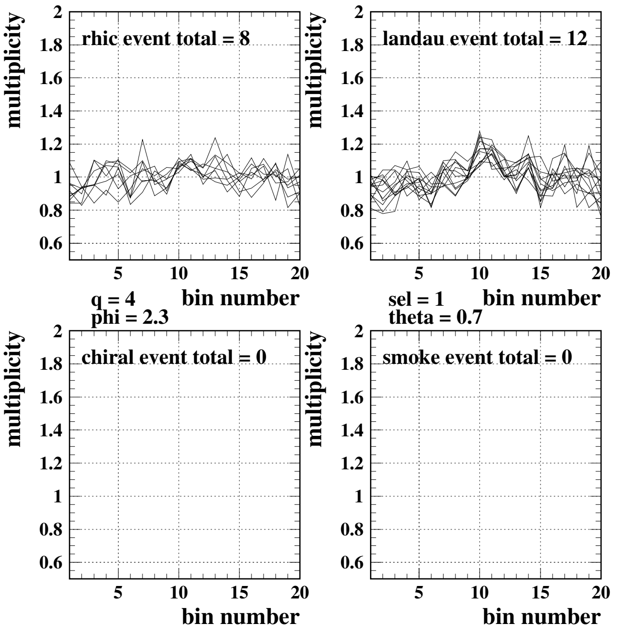

Figure 24: Zone A

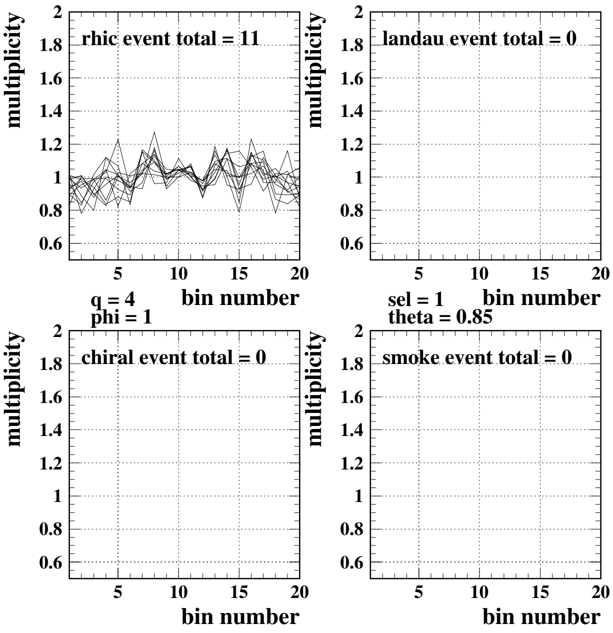

Figure 25: Zone I

Because of the generality of the system we are fairly confident that these analysis techniques exhaust all correlation measurement possibilities.

STAR trigger hardware capability and RHIC event rates limit the amount of computation power and process time available at the various trigger levels. With this work as a reference we can now design optimized algorithms at each level with an understanding of what is being given up and what retained in terms of event selectivity in order to fit the computation envelope.

Beyond the application to trigger algorithm development we also see this correlation analysis system as a central element in the overall STAR data analysis at all stages.

References

[1] Autocorrelation Multiplicity Trigger - One-dimensional Simulations, University of Washington Nuclear Physics Laboratory, T. A. Trainor, Preprint (1993).

[2] Power Spectrum Analysis of Modified HIJET Events, T. A. Trainor, University of Washington Nuclear Physics Laboratory, Preprint (1994).

[3] Power Spectrum Analysis with Nonuniform Bin Size and Variable Bin Number, T. A. Trainor, University of Washington Nuclear Physics Laboratory, Preprint (1994).

[4] On the Scaling Behavior of Topological Measures, T. A. Trainor, University of Washington Nuclear Physics Laboratory, Preprint (1995).

[5] Introduction to STAR Level-2 Trigger Algorithms, T. A. Trainor and J. G. Reid, University of Washington Nuclear Physics Laboratory, Preprint (1995).

[6] HIJET and Beyond, R. S. Longacre, Brookhaven National Laboratory, Preprint (1994).